Evaluating reconstruction algorithms for respiratory motion guided acquisition

To cite this article before publication: Owen Dillon *et al* 2020 *Phys. Med. Biol.* in press https://doi.org/10.1088/1361-6560/ab98d3

Evaluating Reconstruction Algorithms for Respiratory Motion Guided Acquisition

Owen Dillon[1], Paul J. Keall[1], Chun-Chien Shieh[1] and Ricky T. O'Brien[1]

[1] ACRF Image X Institute, Faculty of Medicine and Health, University of Sydney, Sydney NSW 2006, Australia

Abstract

Conventional thoracic 4DCBCT scans take 1,320 projections over 4 minutes. This paper investigates which reconstruction algorithms best leverage Respiratory-Motion-Guided (RMG) acquisition in order to reduce scan time and dose while maintaining image quality.

We investigated a 200 projection, on average 1-minute RMG acquisition. RMG acquisition ensures even angular separation between projections at each respiratory phase by adjusting the imaging gantry rotation to the patient respiratory signal in real time.

Conventional 1,320 projection data and RMG 200 projection data were simulated from 4DCT volumes of 14 patients. Each patient had an initial 4DCT reconstruction, treated as a planning 4DCT, and a 4DCT reconstruction acquired later, used for 4DCBCT data simulation and evaluation.

Reconstructions were computed using the Feldkamp-David-Kress (FDK), McKinnon-Bates (MKB), RecOnstructiOn using Spatial and TEmporal Regularization (ROOSTER), and Motion Compensated FDK (MCFDK) algorithms. We also introduced and evaluated a novel MCMKB algorithm.

Image quality was evaluated with Root-Mean-Square Error (RMSE), Structural SIMilarity index (SSIM) and Tissue Interface Sharpness (TIS). Rigid registration of the tumor volume regions between the reconstruction and the ground truth was used to evaluate geometric accuracy.

Relative to conventional 4DCBCT acquisition, the RMG acquisition delivered 80% less dose and was on average 70% faster. The conventional-acquisition 4DFDK-reconstruction volumes had mean RMSE, SSIM, TIS and geometric error of 94, 0.9987, 2.69 and 1.19mm respectively. The RMG-acquisition MCFDK-reconstruction volumes had mean RMSE, SSIM, TIS and geometric error of 113, 0.9986, 1.76 and 1.77mm respectively with minimal increase in computational cost. These results suggest scan time and dose can be significantly reduced with minimal impact on reconstruction quality by implementing RMG acquisition and motion compensated reconstruction.

Keywords: Thoracic CBCT, Reconstruction, Imaging Protocols, Radiotherapy

1. Introduction

When a thoracic cancer patient is placed in a linear accelerator for radiotherapy, a four-dimensional cone beam CT (4DCBCT) scan is often acquired to align the patient's anatomy on the day of treatment with the anatomy used for the treatment plan. These scans add time and imaging dose to each treatment fraction, so it would be clinically useful to develop shorter scans with fewer projections that produce similar or better reconstructions relative to the standard procedure. We define a "standard" 4DCBCT scan as a "conventional" 1,320 projection 4 minute acquisition with projections retrospectively sorted by respiratory phase [1] and reconstructed with the Feldkamp-Davis-Kress (FDK) [2] algorithm.

This paper investigates and evaluates 4DCBCT scans with alternative acquisition and reconstruction. The Respiratory-Motion-Guided (RMG) [3] acquisition protocol ensures even angular spacing between projections at each respiratory phase by modulating the gantry rotation speed and kV acquisition rate in response to the patient's real-time respiratory signal to increase consistency and reduce redundancy in the data. We reconstruct the RMG data with several algorithms, namely 3DFDK, 4DFDK, McKinnon-Bates (MKB) [4] which uses the 3DFDK reconstruction to correct artefacts in the 4DFDK reconstructions, RecOnstructiOn using Spatial and TEmporal Regularization (ROOSTER) [5] which imposes spatial and temporal structure, and Motion Compensated FDK (MCFDK) [6] which makes use of Deformable Image Registration (DIR) [7] to estimate Deformation Vector Fields (DVFs) that then compensate for the patient motion. Standard MCFDK reconstruction uses DVFs estimated from the planning 4DCT. We introduce MCMKB, where DVFs are estimated from the MKB reconstruction.

Reducing acquisition time and dose is an ongoing topic of study. Earlier work has investigated increasing gantry rotation speed and decreasing total number of projections by up to a factor of 4 [8]. This work found that a factor of 2 gave clinically acceptable image quality when standard reconstruction algorithms were used. Phantom studies using RMG-acquisition and FDK-reconstruction have shown a 54% dose reduction only led to a 6% lower Signal-to-Noise Ratio and 7% lower Contrast-to-Noise Ratio [9].

Reconstruction algorithm research often focuses on both improving image quality from standard acquisition data and image quality for faster, lower dose acquisition [4] [6] [10] [11] [12]. A grand challenge of reconstruction algorithms for 1-minute fixed gantry velocity half-fan acquisition is summarized in [13]. This challenge includes many of the reconstruction algorithms evaluated in this paper, and some that can be interpreted as extensions. This paper investigates RMG full fan acquisition as implemented in [9] to potentially reduce acquisition time and dose further. The use of RMG acquisition ensures the data will not have large angular gaps, which may significantly alter the relative performance of reconstruction algorithms found in [13].

The novel contribution of this paper is the combination of acquisition and reconstruction methods. Our aim is to determine the acquisition and reconstruction combination that minimizes scan time and dose without compromising on image quality or incurring clinically unfeasible computation cost.

2. Method

Conventional and RMG 4DCBCT data were simulated from patient data from the Cancer Imaging Archive (TCIA) 4D-Lung dataset [14]. Each patient had 10 respiratory correlated 4DCT volumes which were used as ground truths. The respiratory phase for each projection angle was calculated, and forward projections with quantum noise simulated through the 4DCT volume of that phase to create 4DCBCT data. The 4DCBCT data were then reconstructed with several algorithms, and image quality metrics were computed relative to the 4DCT ground truth. The conventional-acquisition 4DFDK-reconstruction volumes were used as the baseline for comparison. An overview of the study design is shown in figure 1.

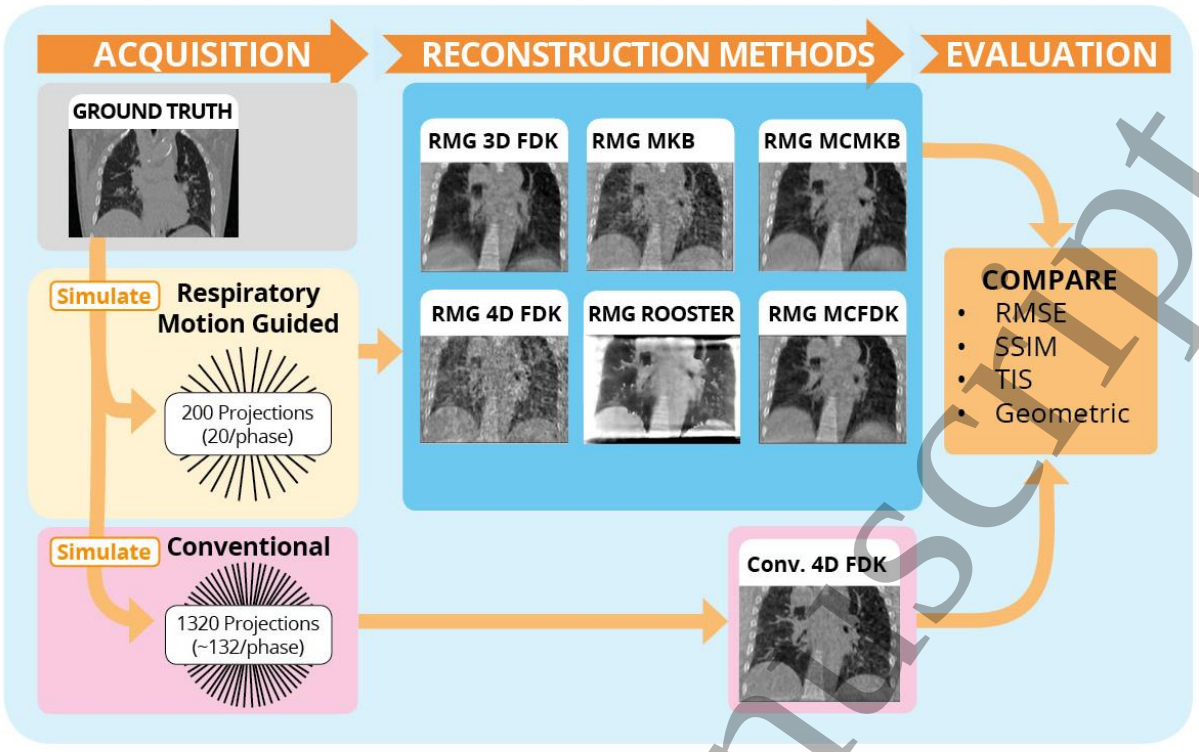

Figure 1: Study design schematic. The 4DCT volumes are used as ground truths for simulating conventional and RMG 4DCBCT acquisitions. The data are then reconstructed with various algorithms and metrics computed using the 4DCT ground truth. The conventional-acquisition 4DFDK-reconstruction is used as a comparison baseline.

A. The Patient Imaging Dataset

The patient image dataset consists of pairs of 10 bin 4DCT scans collected from 14 patients on different days. The other 6 patients in the dataset only had a single 4DCT so could not be used for this study. Each patient had locally advanced non-small-cell lung cancer (NSCLC) and received 3D conformal radiotherapy. The first 4DCT scan was treated as the planning 4DCT, with those volumes available for parameter tuning and motion estimation of the 4DCBCT reconstruction algorithms. The second 4DCT scan was used as a ground truth for 4DCBCT simulation and reconstruction quality quantification. There were 6 to 44 (median 15) days between the "planning" 4DCT scan and "ground truth" 4DCT scan.

B. Simulating Acquisition

The forward and back projections, as well as the reconstruction methods, were implemented using the open source Reconstruction Tool Kit (RTK) [15]. The computational hardware used was a desktop workstation with 64GB of RAM, 32 3.1 GHz CPU cores and 2 Nvidia GPU cards with combined 3,712 CUDA cores and 16GB VRAM. We used a 1,000 mm source-isocenter distance, 1,536 mm source-detector distance, 512 × 512 pixel detector with 1 mm^2 pixels, full fan, 200° arc gantry model.

For the conventional acquisition (1,320 projections, 4 minutes, fixed gantry velocity), cone beam projections were simulated at time t from angle $\theta(t)$ through the j'th respiratory phase 4DCT volume where phase $j(t)$ was computed retrospectively from a recorded patient breathing trace.

Data for a 200 projection RMG acquisition were also simulated. The gantry is rotated in real time to patient respiratory phase to ensure even angular separation [3] so for the 200° arc projections through the j'th respiratory phase 4DCT volume are simulated at $j°$, $(j+10)°$, $(j+20)°$, etc. A 200

projection RMG acquisition with typical linear accelerator gantry speeds takes under 80 seconds on average [9]. The focus on a 200 projection scan is justified in the discussion.

After forward projection, both the conventional and RMG acquisition projections were scaled to 30,000 photon counts and corrupted with Poisson noise to produce typical CBCT signals. Scatter was not simulated as scatter correction is typically performed with machine specific hardware and preprocessing software that is not generalizable and often considered separately to the undersampled reconstruction problem [2] [4] [6] [10] [11] [12]. The results from the AAPM SPARE grand challenge in [13] verify that scatter reduces CBCT absolute image quality, however the impact on relative image quality across CBCT acquisition and reconstruction methods is negligible.

C. Reconstruction Algorithms

We computed FDK reconstructions of the conventional and RMG acquisition data, with conventional-acquisition 4DFDK-reconstruction as the baseline. The RMG-acquisition data were reconstructed with several algorithms as described in figure 1 to evaluate which works best for RMG-acquisition data.

1. Feldkamp-Davis-Kress

Both conventional and RMG acquisition data were reconstructed with the RTK implementation of 3DFDK [2] and 4DFDK [1] algorithms. Standard clinical 4DCBCT practice is conventional-acquisition 4DFDK-reconstruction hence it was used as the comparison baseline. We implemented Hann filtering (rather than ramp filtering) and sinogram padding to bring the FDK reconstructions closer to current clinical implementations rather than the original literature [1] [2] [15]. In 3DFDK reconstruction, every projection is filtered and back projected whereas in 4DFDK reconstruction only those projections acquired at a particular respiratory phase are filtered and back projected.

2. McKinnon-Bates

The RMG acquisition data were also reconstructed with the MKB algorithm [4]. For this algorithm, the 3DFDK and 4DFDK reconstructions were first computed. The respiratory phase j 4DFDK volume was computed from projections acquired at angles θ_j. Projections at angles θ_j were simulated from the 3DFDK volume and reconstructed with FDK to produce a simulated 4DFDK. The simulated phase j 4DFDK volume were subtracted from the true phase j 4DFDK volume to produce a phase j difference volume. The difference volume is scaled and subtracted from the 3DFDK volume to produce the phase j MKB volume. Note that in the original paper, difference projections are used rather than difference volumes. We computed difference volumes as the file structure supported higher numerical precision and signed values, whereas our projections were stored as unsigned integers which could cause overflow issues. Our MKB implementation makes use of Hann filtering and sinogram padding similarly to our FDK implementation. A schematic of our MKB implementation is shown in figure 2.

3. ROOSTER

The RMG acquisition data were also reconstructed with the ROOSTER algorithm [5]. The ROOSTER algorithm iteratively computes volumes that minimizes the sum of the least-squares difference between volume simulated projections and measured projections, and a spatiotemporal "total variation" term that promotes distinct homogenous regions with sharp edges.

4. MCFDK

The RMG acquisition data were also reconstructed with the Motion Compensated FDK (MCFDK) algorithm [6]. Motion was estimated from the planning 4DCT volumes by DIR between respiratory

phase volumes using a B-spline method from the Elastix toolkit [16]. The 4DCT DIR produced DVFs that are used as inputs for MCFDK reconstruction.

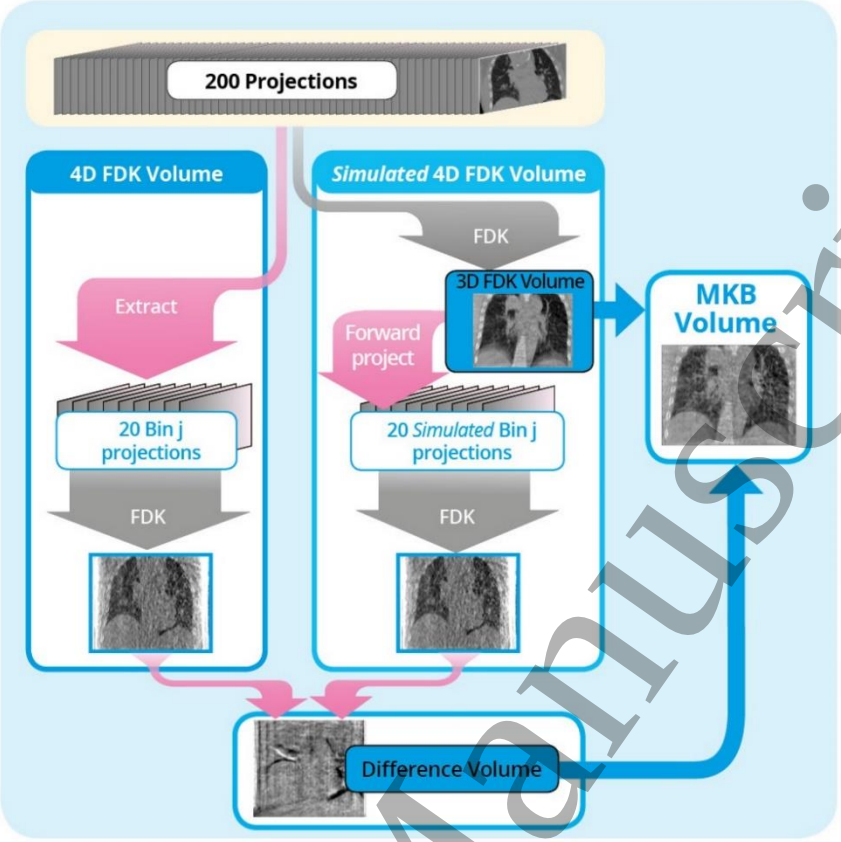

Figure 2: Schematic of the McKinnon-Bates algorithm. The 3DFDK volume and 4DFDK volumes are computed. The 3DFDK volume is used to create simulated 4DFDK volumes, which are then subtracted from the true 4DFDK volumes to produce difference volumes. The difference volumes are added to the 3DFDK volume to produce MKB volumes.

The MCFDK algorithm can be interpreted as a variation of the FDK method where the back projection is performed along curved paths to account for the motion. We implemented the MCFDK method by performing back projection along straight paths, then warping using the DVFs from the planning 4DCT. A schematic detailing our implementation of the MCFDK method is shown in figure 3.

We used peak inhale (respiratory phase bin 6 in our convention) as the "reference frame" as this gave the greatest lung volume for registration. We computed the 9 DVFs from bin *j* to bin 6, and the 9 DVFs from bin 6 to bin *j* for 18 DVFs in total. Note that the DVF computation can be done before the CBCT data are acquired.

When CBCT data were acquired, the 4DFDK reconstructions were computed. The planning 3DCT volume and 3DFDK volume were rigidly aligned, and this alignment applied to the planning 4DCT DVFs. The 4DFDK volumes had the bin *j* to bin 6 DVFs applied, and the resulting 10 volumes were averaged to produce the bin 6 MCFDK volume. The 9 DVFs from bin 6 to bin *j* were then applied to the bin 6 MCFDK volume to produce the remaining 9 volumes of the 4D MCFDK reconstruction. Recall that 6 to 44 (median 15) days pass between the 4DCT scan used for DVF estimation and the 4DCT scan used for 4DCBCT scan simulation and evaluation.

5. MCMKB

The RMG acquisition data were also reconstructed with the Motion Compensated MKB (MCMKB) algorithm. This algorithm is an extension of [11], where 4DFDK reconstructions are used for DVF

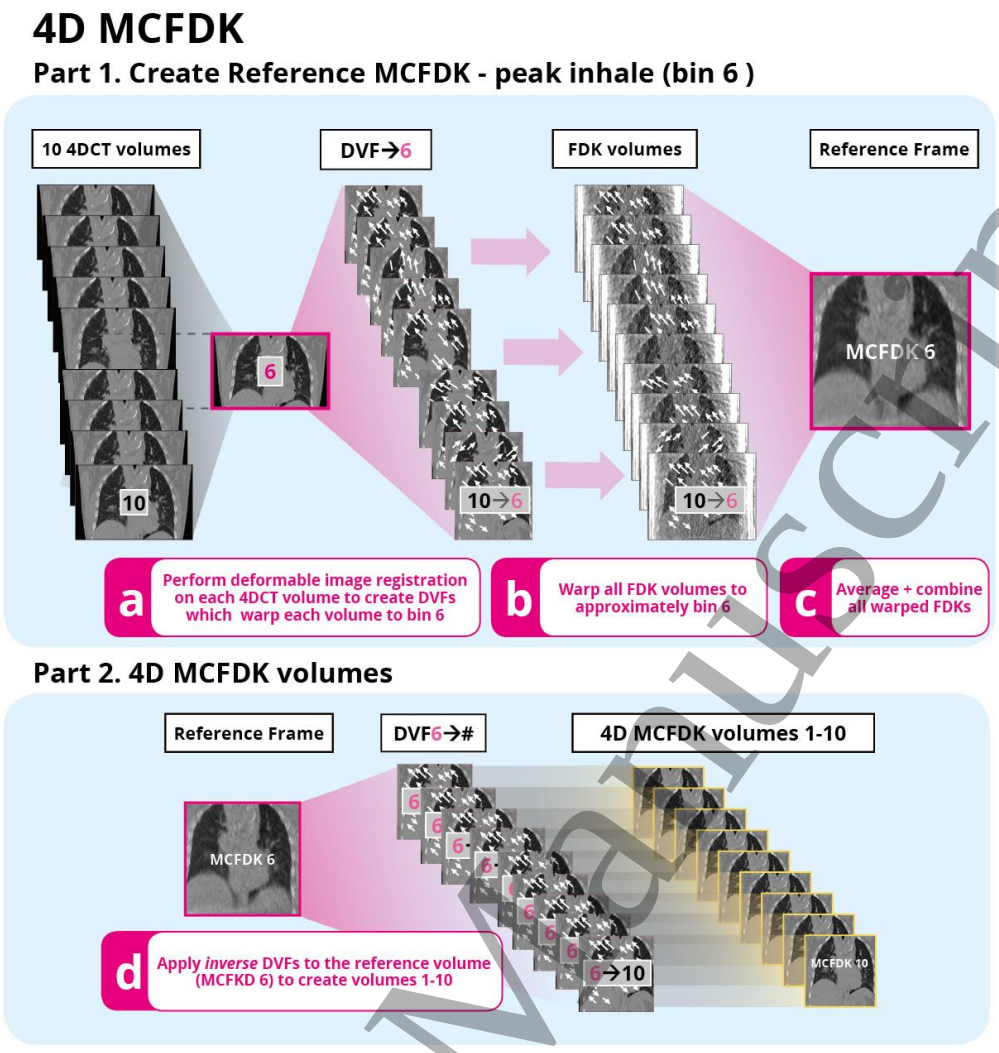

Figure 3: The Motion Compensated FDK (MCFDK) algorithm. DVFs between the respiratory phase bin 6 and bin j 4DCT volumes are estimated by DIR. These DVFs are applied to the corresponding 4DFDK volumes to produce 10 volumes that are averaged to form the bin 6 MCFDK volume. Corresponding inverse DVFs are then applied to the MCFDK bin 6 volume to create the remaining 9 MCFDK volumes.

estimation. This study considers a far more undersampled acquisition than [11], which may explain why we were unable to produce convergent DVF estimates from the 4DFDK reconstructions. We were able to compute convergent estimates of DVFs from the MKB reconstructions, hence the introduction of the MCMKB algorithm. The DVFs estimated from the MKB volumes were used as inputs to the MCFDK algorithm to produce MCMKB volumes.

6. Summary

The reconstruction methods are described below with concise mathematical notation

Method	Mathematical Summary	Notes
3DFDK	$x_{3DFDK} = A^T Fp = \frac{1}{n_b}\sum_{j}^{10} A_j^T F_j p_j$	Standard 3D reconstruction. Demonstrates level of motion.
4DFDK	$x_{4DFDK,j} = A_j^T F_j p_j$	Standard 4D reconstruction.
MKB	$p_{s,j} = A_j x_{3DFDK}$ $x_{s,j} = A_j^T F_j p_{s,j}$ $(\hat{a},\hat{b}) = \min_{a,b}\left\{\left\|a + bx_{s,j} - x_{4DFDK,j}\right\|_2^2\right\}$	Uses forward and back projection in reconstruction. Uses 3D and 4D data in reconstruction.

	$x_{diff,j} = \hat{a} + \hat{b}x_{s,j} - x_{4DFDK,j}$ $x_{MKB,j} = x_{3DFDK} - x_{diff,j}$	
ROOSTER	$x_{ROOSTER,j} = \min_x \left\{ \left\| A_j x - p_j \right\|_2^2 + R(x, x_{k\neq j}) \right\}$ $R(x, x_{k\neq j}) = w_0 TV(x) + \sum_{\substack{k=1 \\ k\neq j}}^{10} w_k TV(x - x_k)$	Iterative method with (total variation) regularization.
MCFDK	$x_{4DCT,r} \approx W_{r,j}(x_{4DCT,j})$ $x_{3DFDK} \approx T(x_{3DCT})$ $x_{MCFDK,r} = \frac{1}{10}\sum_{j=1}^{10} \left(T(W_{r,j})\right)(x_{4DFDK,j})$ $x_{MCFDK,j} = \left(T(W_{j,r})\right)(x_{MCFDK,r})$	Motion compensation from plan CT.
MCMKB	$x_{MKB,r} \approx \widehat{W}_{r,j}(x_{MKB,j})$ $x_{MCMKB,r} = \frac{1}{10}\sum_{j=1}^{10} \widehat{W}_{r,j}(x_{4DFDK,j})$ $x_{MCMKB,j} = \widehat{W}_{j,r}(x_{MCMKB,r})$	Motion compensation from current CBCT.

where x_r denotes a reconstruction with method r, A is forward projection, A^T is back projection, F is filtering, p is a sinogram and subscript j denotes correspondence to respiratory phase bin j. For MKB, $p_{s,j}$ is the simulated sinogram corresponding to projections at phase bin j, $x_{s,j}$ is the FDK reconstruction of the simulated sinogram, $\hat{a}$ and $\hat{b}$ are scaling constants and $x_{diff,j}$ is the bin j difference volume. For ROOSTER, R is the spatiotemporal total variation term, $TV(x)$ is the total variation of x and w_k is the k'th weight. For MCFDK, $x_{4DCT,j}$ is the respiratory phase j 4DCT volume, r is the reference phase, $W_{r,j}$ is the deformation from $x_{4DCT,j}$ to $x_{4DCT,r}$, x_{3DCT} is the 3DCT volume (average of 4DCT volumes), T is the rigid deformation from x_{3DCT} to the 3DFDK volume x_{3DFDK} and $x_{MCFDK,j}$ is the respiratory phase j MCFDK volume. For MCMKB, $\widehat{W}_{r,j}$ is the deformable registration from respiratory phase j MKB volume $x_{MKB,j}$ to respiratory phase r MKB reference volume$x_{MKB,r}$.

The algorithms in this study were selected to be representative of emerging approaches in 4DCBCT reconstruction. For example, Prior Image Constrained Compressed Sensing (PICCS) [10] makes use of total variation regularization as in ROOSTER, but with a total variation term between 4DCBCT and planning 4DCT volumes. Simultaneous Motion Estimation and Image Reconstruction (SMEIR) [12] also utilizes total variation regularization alongside data driven motion compensation as in MCMKB.

D. Image Quality Metrics

Image quality of the reconstructed volumes was quantified. To avoid truncation artefacts impacting the results, metrics were computed over subvolumes contained within the field of view. To ensure the metrics reflect practical interpretability, the voxel values within the subvolumes were automatically affine windowed. Let $X_{GT}, X_r \in \boldsymbol{R}^N$ be ground truth and reconstruction voxel value vectors and let $x_{gt}, \hat{x}_r \in \boldsymbol{R}^n$ be ground truth and reconstruction voxel value vectors from the subvolume where the reconstruction volume contains N voxels and the subvolume contains $n < N$ voxels. The windowed subvolume voxel values are $x_r = \hat{a}\hat{x}_r + \hat{b}$ where $(\hat{a}, \hat{b}) = \min_{a,b}\{\|x_{GT} - ax_r - b\|_2^2\}$. Central slice views of the ground truth 4DCT and 3DFDK volume and subvolumes are shown in figure 4.

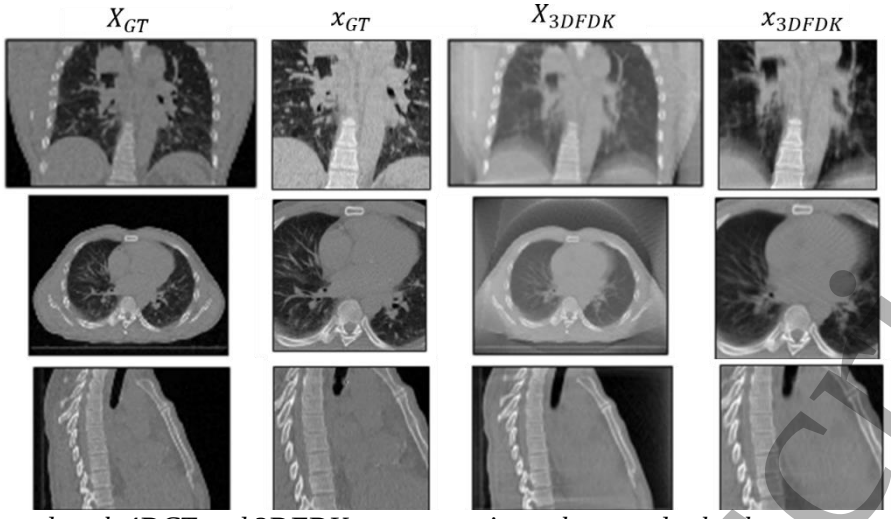

Figure 4: Ground truth 4DCT and 3DFDK reconstruction volume and subvolume tomographs. The left 2 columns show the 4DCT ground truth volume and subvolume. The right 2 columns show 3DFDK reconstruction volume and subvolumes. Note the subvolume is entirely contained in the field of view.

The RMSE and SSIM were computed as

$$RMSE = \frac{1}{\sqrt{n}}\|x_{GT} - x_r\|_2 \qquad SSIM = \frac{(2\mu_{GT}\mu_r + c_1)(2\sigma_{r,GT} + c_2)}{(\mu_{GT}^2 + \mu_r^2 + c_2)(\sigma_{GT}^2 + \sigma_r^2 + c_2)}$$

where μ and σ^2 denote voxel value means and variances, $c_1 = (0.01L)^2$ and $c_2 = (0.03L)^2$ where L is the dynamic range of the volumes.

Reconstruction quality was also quantified with Tissue Interface Sharpness (TIS) as in [11]. A $5 \times 5 \times l$ voxel subvolume was placed at the top of the diaphragm, where $l \approx 50$ is the run length. From the subvolume 25 voxel value runs of length l running in the superior-inferior axis are extracted. Each run is normalized to values from 0 to 1 and a sigmoid fitted. The average sigmoid gradient is the TIS. The TIS was only computed at peak exhale to ensure the diaphragm/lung boundary was sufficiently far from truncation artefacts.

Reconstruction quality was also quantified with "geometric accuracy" as in [13]. A subvolume was placed over the clinician-contoured tumor volume of the ground truth 4DCT volume to form a ground truth subvolume. A subvolume at the same location as the ground truth subvolume was extracted from each reconstruction volume and rigidly registered to the ground truth subvolume automatically in Elastix [16]. The translation and root-mean-square (RMS) rotation estimated by Elastix are the geometric error. Geometric error was calculated on peak exhale volumes as only this phase volume had clinician-contoured tumor volumes available. Geometric error was only calculated for 11 of the 14 patients. For patient 4, the tumor volume was considered too large for centroid estimation to be meaningful. For patient 6, the tumor was largely outside the field of view. For patient 7, no clinician-contoured tumor volume was available.

3. Results

Reconstruction central slice views for patient 1 at peak exhale are shown in figure 5. Coronal views of the tumor subvolumes used for assessing geometric accuracy are shown in figure 7.

Results for RMSE, SSIM and TIS between 4DCBCT acquisition-reconstruction methods for all 14 patients are summarized as boxplots in figure 6. The geometric error translation and rms rotation for 11 patients as described in the methods are shown in figure 8. Note that patient 5 was found to be an outlier with abnormally high geometric error.

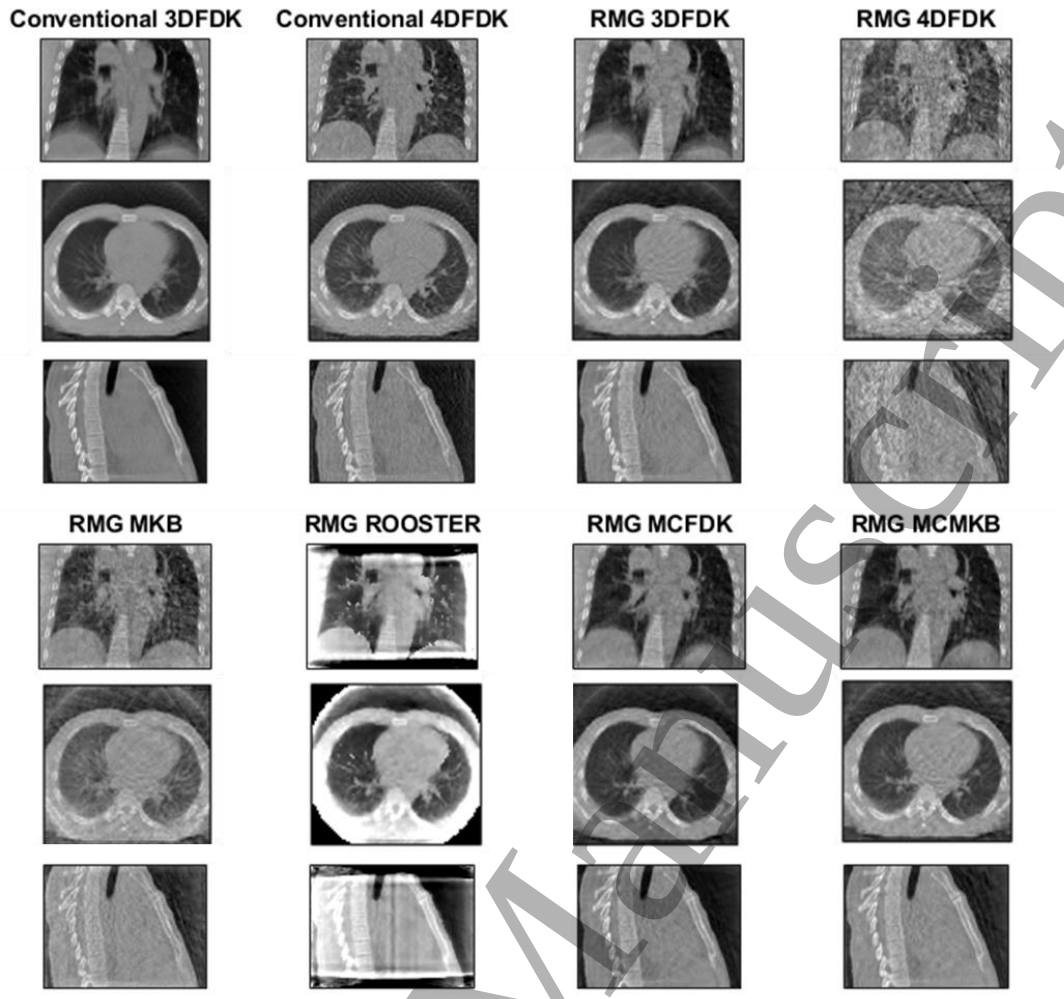

Figure 5: Central coronal, axial and sagittal slice reconstructions of patient 1 at peak exhale for each acquisition/reconstruction 4DCBCT method considered. "Conventional" indicates 1,320 projection fixed gantry velocity acquisition, "RMG" indicates 200 projection RMG acquisition.

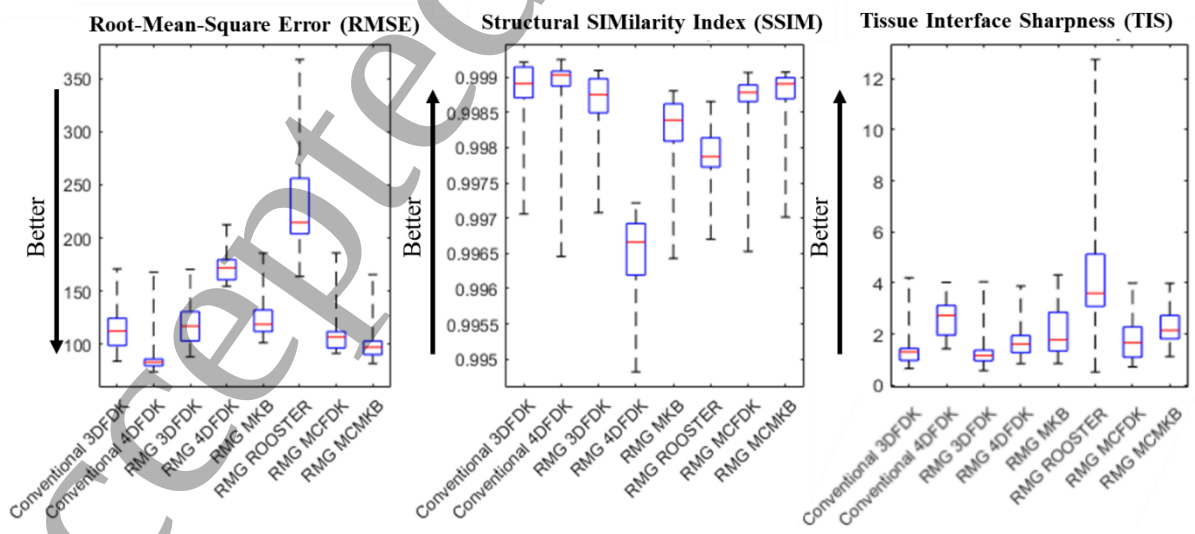

Figure 6: Boxplots of phase averaged RMSE, SSIM and peak exhale TIS for each considered acquisition/reconstruction 4DCBCT methods across all 14 patients. Note that a "better" reconstruction would have lower RMSE, higher SSIM and higher TIS.

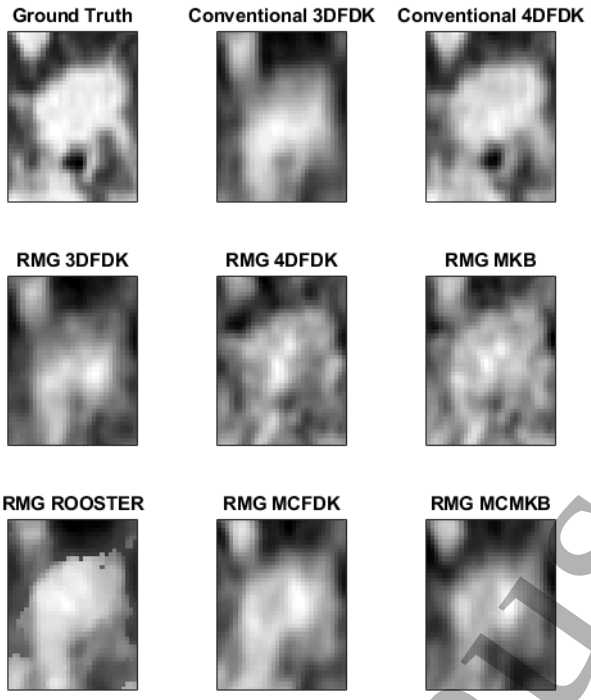

Figure 7: Central axial slice view of patient 1 tumor subvolume. Each subvolume was automatically rigidly aligned to the upper right 4DCT ground truth subvolume to estimate geometric accuracy.

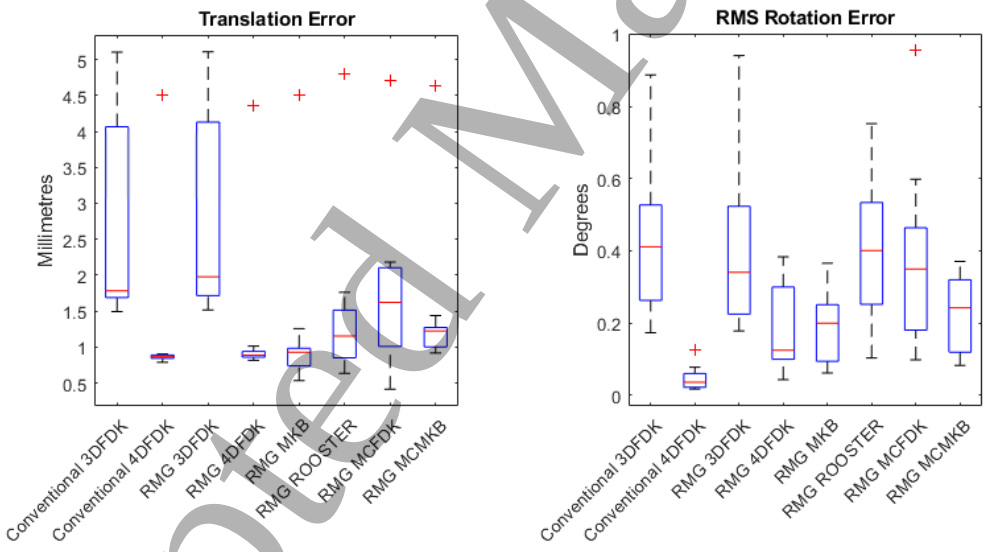

Figure 8: Geometric translation and RMS rotation error boxplots of considered acquisition/reconstruction 4DCBCT methods across 11 patients. The identified outlier is patient 5.

4. Discussion

This study was designed to find the reconstruction method that best leverages RMG acquisition to reduce 4DCBCT scan time and dose while maintaining image quality relative to the standard 4DCBCT conventional-acquisition 4DFDK-reconstruction baseline. We now discuss performance of each acquisition-reconstruction 4DCBCT method. Qualitative features observed in the patient 1 peak exhale volumes shown in figure 5 were found to be consistent across patients and respiratory phases. Quantitative results are shown in figures 6 and 8.

Note that for geometric error, all 4D-reconstruction methods achieved translation errors under 2 millimeters except for patient 5, and all reconstruction methods had RMS rotation below 1 degree. We believe the poor result for patient 5 was due to the automatic registration being biased towards some artefact in the reconstruction. Considering that reconstructions were computed on $1mm^3$ voxels, comparisons between such small translations may not be clinically meaningful. Direct qualitative inspection as in figure 7 may better indicate clinical usefulness.

The conventional-acquisition 3DFDK-reconstruction and RMG-acquisition 3DFDK-reconstruction volumes have clear motion blur at the top of the diaphragm. This is a result of all data being filtered and back projected. The RMG-acquisition 3DFDK-reconstruction volume appears only slightly noisier than the conventional-acquisition 3DFDK-reconstruction volume, despite being computed from only 200 rather than 1,320 projections. This could imply that FDK reconstruction quality for evenly spaced 200° arc full fan projection data saturates at around 200 projections. The conventional-acquisition and RMG-acquisition 3DFDK-reconstruction volumes had similar quantitative performance, and particularly poor TIS and geometric error that is likely due to the motion blur.

The conventional-acquisition 4DFDK-reconstruction baseline volume appears slightly noisier than the conventional-acquisition 3DFDK-reconstruction volume but with almost no visible motion blur. The RMG-acquisition 3DFDK-reconstruction volume appears similarly noisy to the conventional-acquisition 4DFDK-reconstruction volume but with motion blur. The comparable noise level is reasonable when we consider that a conventional-acquisition 4DFDK-reconstruction volume is computed from FDK reconstruction of ~132 projections while a RMG-acquisition 3DFDK-reconstruction volume is computed from FDK reconstruction of 200 projections.

The RMG-acquisition 4DFDK-reconstruction volume appears to have little motion blur but is noisy and with well defined “streak” artefacts visible in the axial view. Streak artefacts are expected in undersampled FDK reconstruction, and a RMG-acquisition 4DFDK-reconstruction volume uses just 20 projections, so the streaking is unsurprising. The volume is at least somewhat interpretable.

Recall that our FDK implementation made use of Hann filtering. The Hann filter parameters were chosen to minimize RMSE and produced volumes with qualitatively lower noise and less well-defined streaks. Sharper (e.g. ramp) filters would result in sharper anatomical boundaries at the cost of additional noise. Given that the 4DFDK reconstructions already have relatively good TIS, the current trade off was considered reasonable. The poor 3DFDK TIS is predominantly due to motion blur.

In our implementation, for RMG-acquisition the 3DFDK-reconstruction and 4DFDK-reconstruction each required approximately 1 minute of computation. Note that in practice, projections can be filtered and back projected during the acquisition. This allows FDK-reconstruction volumes to be available only a few seconds after acquisition completes.

The RMG-acquisition MKB-reconstruction volume appears less noisy and streaky than the RMG-acquisition 4DFDK-reconstruction volume. This is expected, as the streaks in the RMG-acquisition 4DFDK-reconstruction volume and MKB simulated 4DFDK-reconstruction are supposed to overlap

and cancel in the difference volume. Regions with little motion appear similar in the RMG-acquisition 3DFDK-reconstruction volume. This is expected as the difference volume should have low magnitude in these regions. Our implementation of MKB required approximately 2.5 minutes of computation. Note that MKB-reconstruction requires computation of the FDK-reconstruction volumes before the additional simulation-reconstruction-difference steps. The improved RMSE and SSIM for MKB-reconstruction over 4DFDK-reconstruction for RMG-acquisition may make the additional computation time worthwhile, however the TIS and geometric error for MKB-reconstruction seem to have higher variance without clear average improvement.

The RMG-acquisition ROOSTER-reconstruction volume has large homogenous regions with well defined boundaries as expected from a total variation regularized reconstruction. The reconstruction seems poor near and outside the field of view, however the region of interest is typically well contained by the field of view, so truncation artefacts do not impact our analysis. RMSE and SSIM were computed inside the field of view however the ROOSTER-reconstruction volumes performed relatively poorly by these metrics, as well as geometric error. Perhaps further optimization of algorithm parameters e.g. weights and number of iterations would have translated to better performance relative to these metrics. The TIS for ROOSTER-reconstruction volumes was by far the highest, and the sharply defined anatomy may be clinically useful. In our implementation, ROOSTER-reconstruction of RMG-acquisition data computed in approximately 30 minutes. We consider this too slow for current clinical application, but ongoing hardware improvements and further software optimization may make the computational cost clinically feasible in the medium term.

The RMG-acquisition MCFDK-reconstruction volume appears qualitatively similar to the conventional-acquisition 4DFDK-reconstruction baseline volume, but with slightly less noise and slightly more motion blur. The RMG-acquisition MCFDK-reconstruction volume seems most like the RMG-acquisition 3DFDK-reconstruction volume but with reduced motion blur. This is unsurprising, as both the 3DFDK-reconstruction volume and MCFDK-reconstruction volumes are computed with filtered back projection of all acquired projections, however the MCFDK-reconstruction volumes have respiratory phase correlated deformation applied based on the 4DCT volumes. There is a small amount of motion blur visible in the RMG-acquisition MCFDK-reconstruction volume that is likely an effect of the planning 4DCT estimated motion not perfectly matching the true patient motion at the time of 4DCBCT, motivating the use of data-driven reconstruction.

The RMG-acquisition MCFDK-reconstruction volumes significantly outperform the RMG-acquisition 4DFDK-reconstruction volumes and reach similar performance to conventional-acquisition 4DFDK-reconstruction volumes in RMSE and SSIM. The RMG-acquisition MCFDK-reconstruction volumes have slightly better TIS than the RMG-acquisition 4DFDK-reconstruction volumes but slightly worse than the conventional-acquisition 4DFDK-reconstruction volumes. The RMG-acquisition MCFDK-reconstruction volumes may have the worst geometric error of the 4D-reconstruction methods, likely due to the changes in patient respiratory motion between planning 4DCT scan and 4DCBCT scan.

The DVF estimation for MCFDK-reconstruction lasted approximately 2 hours in our implementation. The DVF estimation from planning 4DCT volumes can be computed prior to 4DCBCT acquisition, so this computational cost remains clinically feasible. The only additional post-acquisition computation cost in MCFDK-reconstruction over FDK-reconstruction is rigidly registering the 3DFK-reconstruction volume to the 3DCT planning volume, applying that translation to the 4DCT planning DVFs, and applying those DVFS to the 4DFDK-reconstruction volumes. In our implementation, the computation time after acquisition lasted approximately 2 minutes. We therefore consider 200 projection 1-minute RMG-acquisition MCFDK-reconstruction 4DCBCT a currently clinically viable method should the slight image quality degradation relative to conventional-acquisition 4DFDK-reconstruction prove acceptable.

The RMG-acquisition MCMKB-reconstruction volume is qualitatively similar to the RMG-acquisition MCFDK-reconstruction volume but with less motion blur, likely a result of the data-driven approach. The RMG-acquisition MCMKB-reconstruction volumes slightly outperform the RMG-acquisition MCFDK-reconstruction volumes by all metrics, bringing performance even closer to conventional-acquisition 4DFDK-reconstruction. The DVF estimation took 20 minutes, as a relatively coarse computational grid with relatively few iterations was used in the estimation compared to MCFDK in recognition of the lower quality input data (MKB-reconstruction volumes rather than 4DCT volumes) limiting estimation accuracy, and that computation time is more clinically important in the MCMKB-reconstruction workflow. Further hardware improvements and software optimization could make 200 projection 1-minute RMG-acquisition MCMKB-reconstruction 4DCBCT viable in the near future.

The reconstruction volume image quality would be expected to improve by taking more projections in the RMG acquisition. We initially investigated the 200 projection RMG-acquisition as this would be the same imaging dose to a conventional 3DCBCT scan. The extension to 4D information at the cost of slightly longer acquisition is clinically appealing. The RMG-acquisition 4DFDK-reconstruction volumes were still interpretable, verifying that only an alteration to the acquisition protocol enables extension to 4D information. As discussed above, alternative reconstruction methods with 200 projection RMG-acquisition delivered image quality comparable to the standard conventional-acquisition 4DFDK-reconstruction baseline. We therefore propose the use of 200 projection RMG-acquisition.

5. Conclusion

We have established a 4DCBCT acquisition and reconstruction methodology that produces reconstructions of comparable quality and computational cost at one third of the acquisition time and one sixth of the imaging dose. Relative to the standard 1,320 projection retrospectively binned acquisition with 4DFDK reconstruction as the baseline, we determined that 200 projection RMG-acquisition with MCFDK-reconstruction maintained comparable image quality across the 14 patients considered. While other reconstruction algorithms produced volumes with higher image quality by some metrics, only MCFDK could deliver comparable image quality with clinically feasible computation time on our current hardware. Ongoing improvements in computation hardware and software may allow data driven motion compensation as in MCMKB and regularized iterative reconstruction as in ROOSTER to be clinically viable in the near future.

The next step in reducing CBCT scan time and dose for thoracic cancer patients will be clinical trials involving 200 projection RMG-acquisition with MCFDK and 4DFDK reconstructions. Should the clinicians interpreting and making decisions based on these reconstructions consider the quality acceptable, this work can be translated into improved patient care and throughput. This data can be reprocessed with alternative reconstruction algorithms such as MCMKB to deliver improved image quality as computational improvements allow clinical implementation. The results of this study are encouraging affirmation towards reducing 4DCBCT scan time and dose with current technology.

6. Acknowledgements

This work was supported by NHMRC project grant 1138899. Ricky O'Brien would like to acknowledge the supported of a Cancer Institute New South Wales Career Development Fellowship. We thank Dr Helen Ball for critically reviewing the manuscript, and Julia Johnson for aiding in the creation of figures.

References

[1] J. Sonke, L. Zijp, P. Remeleijer and M. Herk, "Respiratory correlated cone beam CT," *Med Phys,* vol. 32, no. 4, pp. 1176-1186, 2005.

[2] L. A. Feldkamp, L. C. Davis and J. W. Kress, "Practical cone-beam algorithm," *J. Opt. Soc. Am,* vol. 1, no. 6, pp. 612-619, 1984.

[3] R. O'Brien, B. Cooper and P. Keall, "Optimizing 4D cone beam computed tomography acquisition by varying the gantry velocity and projection time interval," *PHYSICS IN MEDICINE AND BIOLOGY,* vol. 58, no. 6, pp. 1705-1723, 2013.

[4] G. McKinnon and R. Bates, "Towards imaging the beating heart usefully with a conventional CT scanner," *IEEE Trans Biomed Eng,* vol. 28, pp. 123-127, 1981.

[5] C. Mory, Cardiac c-arm computed tomography, Universite Lyon, 2014.

[6] S. Rit, J. W. H. Wolthaus, M. v. Herk and J. Sonk, "On-the-fly motion-compensated cone-beam CT using an a priori motion model.," *Med Phys,* vol. 36, pp. 2283-2296, 2009.

[7] S. Oh and S. Kim, "Deformable image registration in radiation therapy," *Radiation Oncology Journal,* vol. 35, no. 2, pp. 101-111, 2017.

[8] A. Bryce-Atkinson, T. Marchant, J. Rodgers, G. Budgell, A. McWilliam, C. Faivre-Finn, G. Whitfield and M. van Herk, "Quantitative evaluation of 4D Cone beam CT scans with reduced scan time in lung cancer patients," *Radiotherapy and Oncology,* vol. 136, pp. 64-70, 2019.

[9] R. O'Brien, U. Stankovic, J. Sonke and P. Keall, "Reducing 4DCBCT imaging time and dose: the first implementation of variable gantry speed 4DCBCT on a linear accelerator," *PHYSICS IN MEDICINE AND BIOLOGY,* vol. 62, no. 11, pp. 4300-4317, 2017.

[10] G. Chen, J. Tang and S. Leng, "Prior image constrained compressed sensing (PICCS): a method to accurately reconstruct dynamic CT images from highly undersampled projection data sets," *Medical Physics,* vol. 35, no. 2, pp. 660-663, 2008.

[11] M. Riblett, G. Christensen, E. Weiss and G. Hugo, "Data-driven respiratory motion compensation for four-dimensional cone-beam computed tomography (4D-CBCT) using groupwise deformable registration," *Med Phys,* vol. 45, no. 10, pp. 4471-4482, 2018.

[12] J. Wang and X. Gu, "Simultaneous motion estimation and image reconstruction (SMEIR) for 4D cone-beam CT.," *Medical Physics,* vol. 40, no. 10, p. 101912, 2013.

[13] C.-C. Shieh, Y. Gonzalez, B. Li, X. Jia, S. Rit, C. Mory, M. Riblett, G. Hugo, Y. Zhang, L. Ren and P. Keall, "SPARE: SPArse-view REconstruction challenge for 4D cone-beam CT from a one-minute scan," *Medical Physics,* vol. 46, no. 9, pp. 3799-3811, 2019.

[14] S. Rit, M. V. Oliva, S. Brousmiche, R. Labarbe, D. Sarrut and G. C. Sharp, "The Reconstruction Toolkit (RTK), an open-source cone-beam CT reconstruction toolkit based on the Insight Toolkit

(ITK)," in *XVII INTERNATIONAL CONFERENCE ON THE USE OF COMPUTERS IN RADIATION THERAPY (ICCR 2013)*, Melbourne, 2013.

[15] S. Rit, J. Nijkamp, M. van Herk and J. Sonke, "Comparative study of respiratory motion correction techniques in cone-beam computed tomography," *Radiotherapy and Oncology,* vol. 100, no. 3, pp. 356-359, 2011.

[16] S. Klein, M. Staring, K. Murphy, M. A. Viergever and J. P. Pluim, "Elastix: a toolbox for intensity-based medical image registration.," *IEEE transactions on medical imaging,* vol. 29, no. 1, pp. 196-205, 2010.

[17] G. Hugo, E. Weiss, W. Sleeman, S. Balik, P. Keall, J. Lu and J. Williamson, "A longitudinal four-dimensional computed tomography and cone beam computed tomography dataset for image-guided radiation therapy research in lung cancer.," *Me Phys,* vol. 44, no. 2, pp. 762-771, 2017.